**Superalloys 2012: 12th International Symposium on Superalloys**
*Edited by: Eric S. Huron, Roger C. Reed, Mark C. Hardy, Michael J. Mills, Rick E. Montero, Pedro D. Portella, Jack Telesman*
***TMS (The Minerals, Metals & Materials Society), 2012***

# Processing to Fatigue Properties: Benefits of High Gradient Casting for Single Crystal Airfoils

Clinique L. Brundidge[1], Tresa M. Pollock[2]
[1]Department of Materials Science & Engineering, University of Michigan, 2300 Hayward St, Ann Arbor, MI 48109, USA
[2]Materials Department, University of California Santa Barbara, Santa Barbara, CA 93106-5050, USA

Keywords: single-crystal nickel-base superalloys, porosity, crack initiation

## Abstract

The fatigue property benefit for higher thermal gradient processing of single crystal superalloys has been evaluated experimentally with two different solidification processing approaches. Low cycle fatigue (LCF) testing was performed at 538°C (R = 0, $f$ = 0.5 Hz) for a René N5 and Ta-modified René N5 alloy solidified with a conventional radiation cooled and higher thermal gradient liquid-metal cooled (LMC) casting process to produce coarse and finer-scaled dendritic structures, respectively. In all specimens tested, cracks initiated at individual pores or large interconnected pores located within the internal volume and near to the surface. Based on statistical analyses of pore size distributions, a model has been developed that predicts the maximum pore size as a function of solidification conditions and the effect of these pores on fatigue life. The model is used to assess the potential property benefits of high thermal gradient processing approaches for a range of cooling rates and component scale sizes

## Introduction

Single crystal nickel-base superalloys have emerged as the structural material of choice for high-temperature applications when significant resistance to fatigue loading is required. Although the fatigue life improvements due to a direct material substitution may be possible, additional gains are achievable through advanced high gradient solidification processing in comparison to typical production processes. A methodology for assessing the potential benefits of new high gradient processes would be useful for assessing their potential in a manufacturing environment. Elliott *et al*. [1] demonstrated significant defect size reduction and dendritic refinement in solidification of large cross-section single crystals via liquid-metal cooling (LMC). Through refinement of defects that can serve as crack initiators, one can expect an improvement to the fatigue property benefits. However, current models that assume a short crack initiation life and predominately focus on crack propagation to estimate the lifetime of a component are not adequate [2,3]. Furthermore, since shrinkage pores are typically the largest flaws within the single crystal casting, it is of critical importance to predict the maximum pore size within a solidified component in order to develop a protocol for characterization that permits fatigue life prediction. To date, metallographic studies of single crystal superalloys report the volume fraction of porosity within a casting and disregard the maximum size and distribution. The maximum defect size is typically assessed by systematic metallographic sectioning or by radiography techniques. Unfortunately, these methods can be time consuming, costly and lack sufficient levels of resolution, particularly for large cross section castings.

The objective of this research is to develop a processing-structure fatigue property model useful for a range of cooling rates, processes, scale sizes and alloy composition. The low cycle fatigue (LCF) property benefits were assessed for coarse and finer-scaled microstructures solidified with a range of solidification rates, for the purpose of identifying the critical relationships between cooling rates and fatigue life. A means of predicting the maximum shrinkage pore size in a given large volume of single crystal material, which may be incorporated into a mechanical property model, was developed.

## Experimental Procedures

Laboratory-scale cylindrical bars of a René N5 (Ni-7.5Co-7.0Cr-1.5Mo-5W-6.5Ta-6.2Al-3Re-0.15Hf-0.05C, wt%) and a modified René N5 (Ni-7.5Co-7.0Cr-1.5Mo-5W-9.3Ta-5.2Al-3Re-0.15Hf-0.05C, wt%) single-crystal nickel-base superalloy were solidified by both a conventional Bridgman and an LMC process in order to produce microstructures with an average secondary dendrite arm spacings, $\lambda_2$, of ~65 μm and ~25 μm, respectively [4]. Heat-treated bars were machined into threaded uncoated specimens and subjected to strain-controlled LCF testing at 538°C until failure using a computer controlled servohydraulic testing system. A triangular load vs time waveform was used with a frequency of 0.5 Hz for the first 24 hours, followed by 9 Hz to failure. The nominal loading axis was in the [001] crystal growth direction. The LCF tests were performed in air at total strain-ranges, $\Delta\varepsilon_t$, between 0.6 and 1.1%.

Fracture surfaces were observed by scanning electron microscopy (SEM) in order to observe the features responsible for initiation. The maximum defect size within the single crystal material was predicted for each variant using statistics of extreme value (SEV) analysis, with the procedure described by Murakami and co-workers [5,6].

## Results

The results of the LCF testing are presented in Figure 1, where the applied alternating stress is plotted as a function of the number of cycles to failure for the four variants. The specimens with a $\lambda_2$ of ~25 μm exhibited up to a 7-fold increase in fatigue life in comparison to the coarser microstructure ($\lambda_2$ = 65 μm) solidified with the conventional cooling process. Cracks initiated from casting pores for all testing conditions, at internal or near-to-the surface locations; examples are shown in Figure 2. The method for differentiating between near-to-surface and internal pores has been described by Murakami [7] by using an equivalent circular diameter, $d$ (Eq. (1)), measured from [001] projected areas, and corresponding (pore) site distance from the surface, $t$. Specifically, if $d/t \geq 1.6$, the pore was determined as a near-to-surface pore; if $d/t < 1.6$, the pore was determined as an internal location.

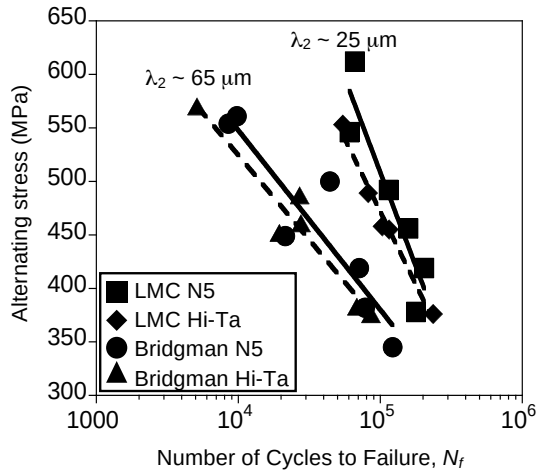


Figure 1. S-N curves for investigated alloys tested at 538°C, $R$ = 0, $f$=0.5 Hz. The LMC data points represent bars solidified with a 12.7 mm/min withdrawal rate, whereas, Bridgman solidified material was cast at 3.4 mm/min.

$$d = \sqrt{\frac{4 * Area}{\pi}} \tag{1}$$

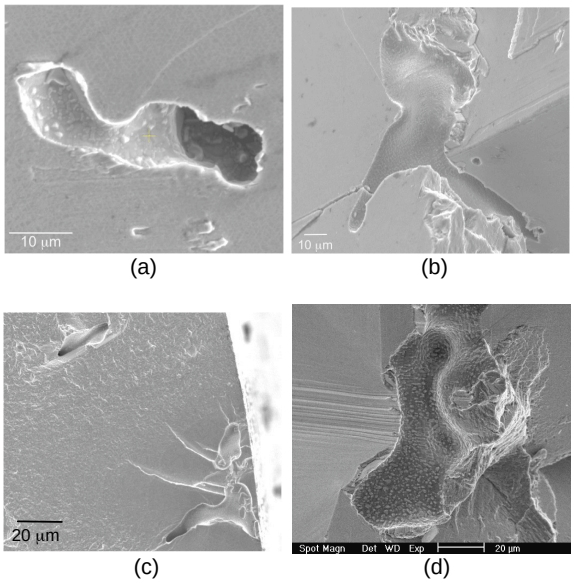


Figure 2. Typical pores from which fatigue cracks initiated. (a) A smaller pore developed during the LMC process initiated cracking from an internal location ($\sigma_{ALT}$ = 455 MPa, $N_f$ = 115,442 cycles). (b) An irregular shaped pore, nucleated during Bridgman solidification, initiated fatigue cracking ($\sigma_{ALT}$ = 382 MPa, $N_f$ = 78,180 cycles); (c) multiple casting pores initiated fracture near the surface ($\sigma_{ALT}$ = 452 MPa, $N_f$ = 19,497 cycles), and slip offsets.

Pore shapes were also characterized by using an aspect ratio (shape factor), $F$, which is a function of the largest diameter, $d_{max}$, and smallest diameter, $d_{min}$, orthogonal to it, as shown below as

$$F = d_{min}/d_{max} \tag{2}$$

An aspect ratio of 1 represents a circular pore in the plane of analysis, while values closer to 0 denote irregular shapes. Table 1 summarizes selected initiation site sizes and aspect ratios for the conditions tested. The single crystal samples processed by LMC initiated cracks at the smaller pores and largest aspect ratios, whereas, more irregularly shaped, larger pores initiated cracks in the coarser material, which significantly reduced the fatigue life. A magnified view of surface intrusions and extrusions near a crack initiating pore site within a Bridgman solidified sample is shown in Figure 2d. Since the initiation process near pores occurs due to the stress concentration, which locally enhances the dislocation processes [8], the surface relief can be attributed to the reversible and irreversible dislocation motion along slip planes. This surface topography causing a geometrical stress concentration is the likely process for crack initiation.

Table 1. Range of pore sizes for each variant.

| Processing Condition | Alloy | Max Site Diameter (μm) | Min Site Diameter (μm) | Shape Factor ($F$) Range |
|---|---|---|---|---|
| LMC | René N5 | 32 | 15 | 0.19-0.69 |
| LMC | Hi-Ta | 38 | 20 | 0.12-0.41 |
| Bridgman | René N5 | 73 | 36 | 0.10-0.29 |
| Bridgman | Hi-Ta | 99 | 62 | 0.03-0.24 |

In six samples, initiation sites were composed of adjacent pores, which initiated cracks in the Bridgman solidified material. One such case is shown in Figure 2c for the initiation site at a near-to-surface location. Adjacent pores are defined as having an edge distance no greater than the $\lambda_2$ for the material. This type of pore configuration produced the largest site sizes measured and are especially detrimental to the fatigue life given that they amplify the stress intensity within the pore site vicinity. Rarely will these defect sizes be observed in metallographic sections and consequently poses a challenge for predicting maximum site sizes in single crystal components.

Pore Population and Fatigue

Since cracks initiate at the largest pores, SEV analysis was performed on metallographically prepared as-cast material. Pore data was acquired from random sections of the single crystal using an inspection area of $S_0 = 2.79 \times 10^{-1}$ mm$^2$ to gather at least 3,000 pores per alloy/process variant. Figure 3 demonstrates that the pores follow a lognormal distribution, allowing the largest pore to be estimated for a predicted volume, $V$ [9].

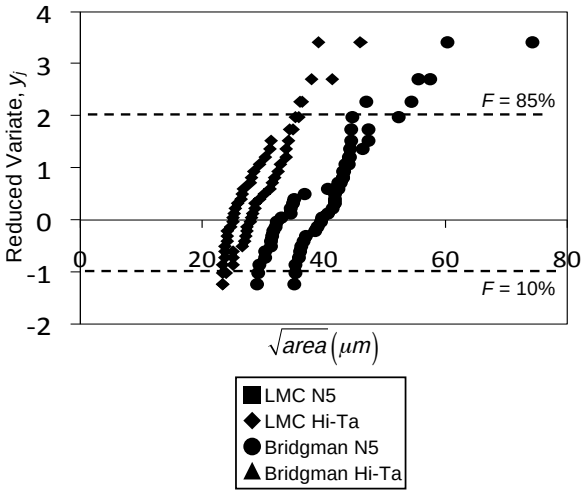


Figure 3. Extreme distribution of pore sizes measured from inspection area, $S_0 = 2.79 \times 10^{-1}$ mm$^2$.

The $y$-ordinate is presented in terms of the the $-\ln(-\ln(F(x)))$, where $F(x)$, the cumulative probability function (CDF) is given as

$$F(x) = \frac{j \times 100}{n+1}(\%) \tag{3}$$

with $j = 1 \ldots n$. The sampled pores are indexed by $j$ to $n$ starting with the smallest defect area:

$$y_i = -\ln\left[-\ln\left(\frac{j}{n+1}\right)\right] \tag{4}$$

Only data contained between the dashed lines are within the confidence bounds for the lognormal distributions, according to the requirements of Gumbel plots [6]. As expected the smaller pores were measured within the LMC material, with up to a 65% reduction in maximum pore size in comparison to the Bridgman solidified material. When comparing the Ta-modified alloy to René N5, there was a marked difference in observed maximum pore size, as well as carbide content (Figure 4). Yet, similar fatigue lives were observed in both alloys at all stress levels tested.

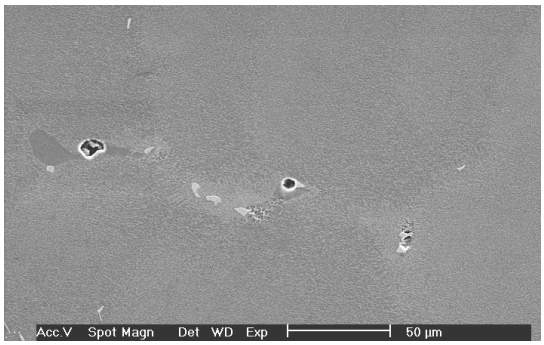


(a)

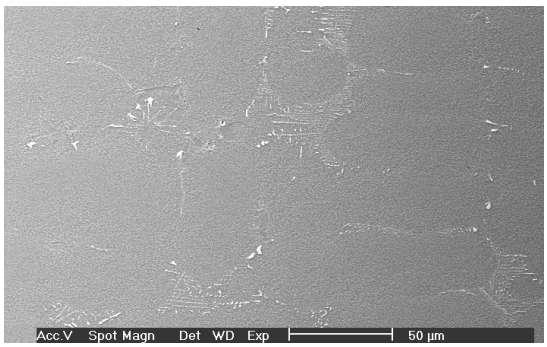


(b)

Figure 4. Secondary electron images of carbides within a (a) Bridgman solidified René N5 alloy, and (b) LMC solidified modified-Ta René N5 alloy.

In order to predict the $\sqrt{area}_{\max}$ of casting pores contained in a given volume, the inspection domain should be in 3-D rather than 2-D. A proposed method shown by Murakami and Toriyama [9] generates a volume by giving a certain thickness to a 2-D area. The standard inspection volume is then describes as $V_0 = h \times S_0$, where $h$ is the thickness. The extreme distribution shown in Figure 3 enables one to predict the maximum casting defect size in a fatigue specimen gage section using an $h$ of 1.9 cm. The return period, $T$, can be calculated for a gage volume equal to 389 mm$^3$ for a fatigue specimen, where

$$T = \frac{V + V_0}{V_0} \tag{5}$$

The predicted defect sizes presented in Figure 5, along with fatigue crack initiating pore size diameters, are shown for comparison. Instead of treating crack initiation sites as one equivalent circular diameter, adjacent pores were measured separately.

The disparity observed between the predicted and actual initiation site size within the Bridgman solidified alloys is likely due to the large mutually interconnected cluster of pores that initiated cracks during fatigue (Figure 2d), yet were separately measured with metallography. The largest initiation site diameter totaled to 99.5 µm, which was from three interconnected pores (42 µm, 61 µm and 65 µm) within a Hi-Ta modified alloy produced with Bridgman casting.

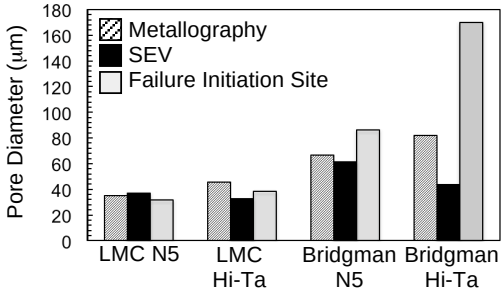


Figure 5. Predicted fatigue initiation site diameters using a statistics of extremes methodology, along with comparisons to maximum pore diameters acquired from distributions of 2,000 pores per variant.

Prediction of Fatigue Life

It is of particular interest to investigate whether the fatigue crack growth stage dominates for a given pore size since the fatigue life decreases with increasing pore area for a given stress level. Typically, the crack initiation life has been considered negligible and the total fatigue life has been estimated by integrating the Paris-Erdogen law, and/or using a small-crack based growth law from the initiation pore size to the final crack size determined by the material's fracture toughness [10]. Using a damage tolerance approach, the application of fracture mechanics can be assessed through Eq. (6) of the form [10]

$$\frac{da}{dN} = C(\Delta K)^m \tag{6}$$

where $da/dN$ is the rate of crack propagation, $C$ and $m$ are constants of $10^{-11}$ MPa$^{-3.6}$-m$^{-1.81}$ and 3.6, respectively, for single crystal René N5 tested at 550°C in air [11]. The $\Delta K$ ($=Y\Delta\sigma(\pi a)^{0.5}$) is the stress intensity factor, $a_o$ is the initial flaw size taken as the fatigue crack initiating pore radius, and $a_f$ is the final crack length. Integration of this equation provides the residual lives of specimens:

$$N_f = \frac{1}{C\Delta\sigma^m Y^m \pi^{m/2}}\left[\frac{2a_0^{1-m/2} - 2a_f^{1-m/2}}{m-2}\right] \tag{7}$$

where m ≠ 2. Table 2 displays the predicted lives based on the crack growth equation, and are shorter than the experimentally measured fatigue lives. This suggests that initiation does not occur immediately during cycling and the crack initiation life dominates the total life.

Table 2. Lifetime data for selected LCF (538°C, $R$ = 0) specimens compared to model predictions using the Paris-Erdogan relation.

| Material | $\sigma_{ALT}$ (MPa) | $a_o$ (μm) | Predicted Life | Actual Life |
|---|---|---|---|---|
| Bridgman N5 | 551 | 27.1 | 1,489 | 9,763 |
| Bridgman Hi- | 570 | 44.2 | 715 | 5,135 |
| Bridgman N5 | 551 | 19.4 | 1,750 | 8,499 |
| Bridgman N5 | 448 | 25.2 | 1,488 | 21,410 |
| Bridgman Hi- | 448 | 36.6 | 836 | 19,497 |
| LMC N5 | 546 | 14.6 | 2,489 | 60,724 |

Since LCF lives were pore size limited, stress intensities at initiation sites are considered. Based on the defect sizes, the initial stress intensity factor, $K_I$, was calculated using the following formulae [5]

$$K_I = 0.65\sigma\sqrt{\pi\sqrt{A_{defect}}} \tag{8}$$

for surface crack initiation, and

$$K_I = 0.5\sigma\sqrt{\pi\sqrt{A_{defect}}} \tag{9}$$

for internal crack initiation, where $\sigma$ is the stress range applied and $A_{defect}$ is the area of the pore measured from a projection on a plane perpendicular to the stress axis. Examples of surface and internal pores are shown in Figure 2. Modification of these equations to account for an initial Mode II stress intensity factor, $K_{II}$, is shown as

$$K_{II} = Y\tau\sqrt{\pi\sqrt{A_{defect}}} \tag{10}$$

where $Y$ equals 0.5 or 0.65 for internal or near-to-surface initiations, respectively, and $\tau$ is the shear stress range. For the purpose of initially developing a simple model describing the role of defect size on fatigue life, the initial stress intensities associated with small cracks emanating from pores were determined for pore sizes observed on post-fatigued specimens. Pore shape is not considered in the subsequent analyses since pore geometry influences the stress intensity by less than 10% [5, 12-14]. Figure 6 displays the relationship between stress intensity using Eqs (8)-(10) and the number of cycles to failure, where open symbols represent near-to-surface initiations. For the four alloy/process variants analyzed, the lives decreased with an increase in initial stress intensity. In the LMC-processed alloys, the stress intensities were far below the $\Delta K_{th}$ of René N5 [11], represented by the dashed line in the figure, in contrast to the coarser solidified material. Yet, damage initiation and crack growth that scaled with the cyclic stress intensity still occurred, leading to failure. It should be noted near-to-surface initiations, which created initial stress intensity values near or greater than $\Delta K_{th}$, produced shorter lives in comparison to internal fractures. Interestingly, near-to-surface initiations occurred at intensity values near or greater than the threshold. The data presented in Figure 6 can be represented by the following power-law relationship:

$$N_T = 2.4\times10^6\left(\Delta K\right)^{-2.4} \tag{11}$$

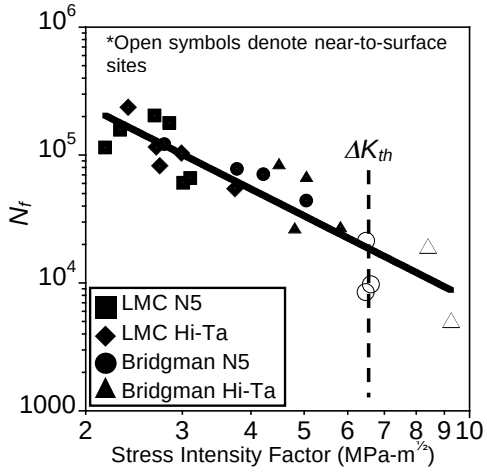


Figure 6. Stress intensities plotted for LMC and Bridgman solidified René N5 and modified René N5 alloys from LCF testing at 538°C.

From Eq. (11), it is evident that there is a dependence of crack initiation and crack propagation on stress and flaw size. When the maximum pore size and the stress level are known, this relation should be useful for predicting the fatigue life. The correlation should break down when the pore sizes are on the same order of magnitude of the microstructural features, such as the dendritic spacings (>150 μm) [4], causing immediate crack initiation. Since

there is a relationship between pore diameter $\lambda_2$, shown in Figure 7 [4], it is possible to incorporate solidification data into Eq. (11) in order to connect to the processing conditions. Eq. (12) describes the dependence of maximum pore size and $\lambda_2$ for various solidification rates, where $d_{pore}$ is the maximum pore diameter measured from metallographic sections as

$$d_{pore} = 1.15\lambda_2 \tag{12}$$

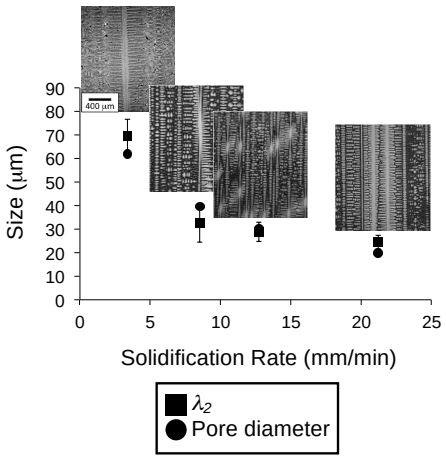


Figure 7. Dependence of maximum pore size and $\lambda_2$ on withdrawal rate for the LMC solidified bars at 8.5-21.2 mm/min and Bridgman cast bars at 3.4 mm/min. Each $\lambda_2$ data point represents a total average measurement obtained only from nearby pore locations.

Solidification experiments have validated that the $\lambda_2$ is related to the cooling rate ($G \times V$) and subsequent coarsening, which is equal to the thermal gradient ($G$) × solidification rate ($V$) as [15]:

$$\lambda_2 \propto (G \times V)^{-1/3} \tag{13}$$

For this reason, the $\lambda_2$ should be a reliable indicator of the overall cooling rate, thermal conditions and maximum defect size that limits the fatigue life, particularly in high gradient growth processes such as LMC. Using the micromechanical model and Eq. (12), the fatigue life, $N_T$, can be represented as

$$N_T = 2.4 \times 10^6 \left( Y \Delta\sigma \sqrt{A\pi (1.15\lambda_2)^{0.95}} \right)^{-2.4} \tag{14}$$

where $A$ is the scaling coefficient for pore-pore interaction, which was found to lie between 1.5 and 2. The scaling coefficient was ascertained by measuring the ratios of maximum to minimum pore areas for interconnected pores at the crack initiation site

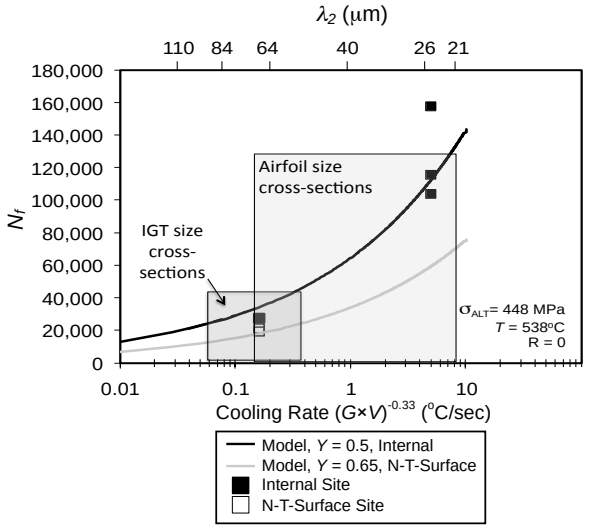


Figure 8. Fatigue life as a function of cooling rate for $T$ = 538°C, $R$= 0 applied to single crystal superalloys. Geometric parameter, Y, is 0.5 and 0.65 for internal and near-to-surface sites, respectively.

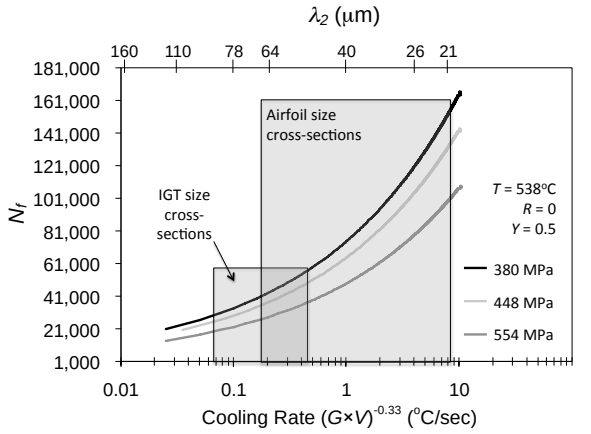


Figure 9. Predicted LCF life ($T$ = 538°C, $R$ = 0) as a function of cooling rate for various stress levels. Curve generated for internal initiation sites only, $Y$ = 0.5.

In order to assess the benefits of high gradient casting for a range of scale sizes, i.e. larger-scale industrial gas turbine (IGT) blades for power generation versus small-scale airfoils, the fatigue life is presented as a function of cooling rate for specific conditions: $T$ = 538°C, $R$ = 0, $Y$ = 0.5. Shaded regions identify the $\lambda_2$ range for large Industrial Gas Turbine (IGT) components and the target scales to airfoils. A substantial benefit to the fatigue life is not expected at $\lambda_2 \leq$ 18 µm for the conditions investigated. Additionally, at this range of refinement, carbides would reside as the largest stress-concentrating defect in the material, rather than pores.

## Discussion

When the fatigue lifetime of single crystal component is critical, design decisions and subsequent system maintenance require information on the bounds for maximum, minimum and average properties. The fatigue model developed here suggests a critical role for solidification processing and the associated pores that result from volumetric shrinkage of the final liquid to solidify. Reducing the maximum pore size to a level that yields the initial stress intensity far below the threshold for a given single crystal material will result in substantially longer initiation lives and less variability in fatigue life. Since the crack initiation process exhibited in these alloys is controlled by localized cyclic plastic deformation, one can expect the largest pores to enhance the local cyclic slip processes to the greatest degree, even below the long-crack cyclic threshold stress intensity. Slip offsets, such as those shown for the near fatigue crack initiating surface pores in the René N5 specimen solidified with the Bridgman process (Figure 2d), provide evidence of the irreversible deformation processes that occur in the vicinity of pores within the bulk as well as within the vicinity of the surface. For a given alternating stress, a critical number of cycles, $N_{crit}$, will be required to develop the necessary surface topography to initiate cracking [16]. Such slip step evidence could further be used to estimate the crack initiation life [17,18] and provide a more mechanistic expression that combines short and long crack models to estimate the total life. The temperature dependence of the fatigue crack initiation process also requires a comprehensive assessment in order to generalize models to a wider range of fatigue test conditions. The modeling here suggests, however, that it is critical to connect the micromechanical models to process models, since each single crystal component experiences different solidification processing conditions, and therefore, different flaws sizes and resultant fatigue life.

From the fatigue and solidification data presented, it is clear that adjusting the processing conditions to prevent formation of interconnected pores, which is due to the dendritic structure and tortuous fluid flow path, would be beneficial. The larger pores present in the Hi-Ta material suggest that the presence of structurally intricate Ta-carbide networks in the interdendritic area (Figure 4) impede the fluid flow in the dendritic channels during solidification. Indeed, carbon additions and the presence of carbides are known to reduce the propensity for convective instabilities and freckle formation [19]. However, carbides with script morphologies that form later in solidification unfortunately create larger pores and apparently also a higher frequency of adjacent pores [20] in comparison to the base alloys. The effect of Ta was especially prevalent in Bridgman casting, where 83% of the specimens initiated cracks from interconnected pores, leading to higher amounts of plastic strain intensification and shorter lives. Rarely will these defect sizes be observed in metallographic sections, which pose a challenge for predicting maximum pores in as-received material using the SEV approach.

The processing-structure-fatigue property model presented in Figure 8 demonstrates the benefits of high gradient casting on the total fatigue life, when the maximum pore size correlates to the scale of the dendritic spacings. This micromechanical model demonstrates the feasibility of linking effects of microstructure variability on the cyclic plasticity scale of the intrinsic microstructure of a single crystal superalloy. A higher thermal gradient process that further refines the $\lambda_2$ and pore size will shift the curves towards longer lives and reduced variability. By utilizing the $\lambda_2$, one would have the capability of estimating specific stress levels that would initiate cracks after a specific lifetime. Following this logic, specific $\lambda_2$ values can be targeted for various regions of the blade during solidification, such as the tip, blade, platform and root.

## Conclusions

Up to a 7X improvement in LCF life at 538°C (R = 0) was produced in small-scale single crystal bars solidified with a higher thermal gradient LMC casting process in comparison to the conventional Bridgman process. A range of casting pore sizes, either near the specimen surface or in the interior, was found to be responsible for crack initiation in all tested specimens, and produced intense strain localization during fatigue.

Actual fatigue crack initiation site diameters were in reasonable agreement with predicted sizes using a SEV approach, with the exception of interconnected pores, which were under predicted by up to a factor of 3. Interconnected pores were only present in the coarser Bridgman solidified material and developed more frequently in the Hi-Ta modified material, which contained intricate script morphologies.

A processing-microstructure-fatigue relationship was derived based on the strong influence of stress range and pore size on the LCF life. The strong correlation between pore size and $\lambda_2$ allows for fatigue property lifetime estimates for a range of cooling rates and component scale sizes. The ability to cast components with shrinkage pore sizes far below the long-crack cyclic threshold of the material will allow for more cycles to initiate cracks during the fatigue process. Modeling of the selected stress levels determined that up to a 10X increase in fatigue life can be obtained using high gradient casting when shrinkage pores are the dominant flaw in the material.

## Acknowledgements

The authors acknowledge the assistance of C.J. Torbet. The funding provided by General Electric Aviation (GE-USA Program) is also gratefully acknowledged.

## References

1. A.J. Elliot, GB. Karney, M.F.X Gigliotti, and T.M. Pollock, “Issues in Processing by the Liquid-Sn Assisted Directional Solidification Technique”, Superalloys 2004, eds. K.A. Green, et al. (Warrendale, PA: The Minerals, Metals and Materials Society, 2004), 421-430.

2. M.D. Miller, P.A.S. Reed, M.R. Joyce, M.B. Henderson, J. Brooks, I.M. Wilcock, “Effect of environment on notch fatigue resistance of CMSX4”, Mater. Sci. Tech., 23 (2007), 1439-1445.

3. N.K. Arakere and J. Moroso, “Fatigue Failure in High-Temperature Single Crystal Superalloy Turbine Blades”, High Temp. Mater. Processes, 20 (2001), 117-135.

4. C.L. Brundidge, D. Van Drasek, B. Wang, T.M. Pollock, “Structure Refinement by a Liquid Metal Cooling Solidification Process for Single-Crystal Nickel-Base Superalloys”, Met. Mat. Trans., 43A (2011), 965-976.

5. Y. Murakami and M. Endo, “Efects of defects, inclusions and inhomogeneities on fatigue strength”, Int. J. of Fat., 16 (1994) 163-182.

6. E.J. Gumbel, Statistics of Extremes, (New York: NY: Columbia University Press, 1958), 80.

7. Y. Murakami, Metal Fatigue: Effects of Small Defects and Nonmetallic Inclusions, (Oxford: Elsevier Science, 2002), 75-118.

8. P. Lukas and L. Kunz, “Slip localisation and fatigue crack initiation in fcc single crystals”, Mater. Sci. Eng. A314, 2001, 75-80.

9. Y. Murakami, T. Toriyama, and E.M. Coudert, “Instructions for a new method of inclusion rating and correlations with the fatigue limit”, J. Testing and Evaluation, 22 (1994, 318-326.

10. P.C. Paris and F. Erdogan, “A critical analysis of crack propagation laws”, J. of Basic Engr., 85 (1963), 528-534.

11. C. Yablinsky, “ Characterizing Fatigue Mechanisms in Ni-Based Superalloys”, PhD Thesis, (Columbus, OH: The Ohio State University, 2010), 50-87.

12. J.-Y. Buffière, S. Savelli, P.H. Jounweau, E. Maire, and R. Fougères, “Experimental study of porosity and its relation to fatigue mechanisms of model Al-Si7-Mg0.3 cast Al alloys”, Mater. Sci. Eng., A316, (2001), 115-126.

13. Y.X. Gao, J.Z. Yi, P.D. Lee, and T.C. Lindley, “A micro-cell model of the effect of microstructure and defects on fatigue resistance in cast aluminum alloys”, Fat. Fract. Eng. Mater. Struct., 27 (2004), 559–70.

14. K. Gall, M.F. Horstemeyer, B.W. Degner, D.L. McDowell, and J. Fan, “On the driving force for fatigue crack formation from inclusions and voids in a cast A356 aluminum alloy”, Int. J. Fract., 108 (2001), 207–33.

15. W. Kurz and D.J. Fisher, Fundamentals of Solidification, (Enfield, NH: Trans. Tech. Publications, 1998), 80-87.

16. H. Mughrabi, “ On ‘multi-stage’ fatigue life diagrams and the relevant life-controlling mechanisms in ultrahigh-cycle fatigue”, Fat. Fract. Engng. Mater. Struct., 25 (2002), 755-764.

17. K. Tanaka and T. Mura, “A dislocation model for fatigue crack initiation”, ASME J. Appl. Mech., 48, 1981, 97-103.

18. K. Tanaka and T. Mura, “ A theory of fatigue crack initiation at inclusions”, Metall. Mater. Trans., 13A (1982), 117-23.

19. T.M. Pollock and S. Tin, “Nickel-based superalloys for advances turbine engines: chemistry, microstructure, and properties”, J. of Prop. Power, 22 (2006, 361-74.

20. K.A. Al-Jarba and G.E. Fuchs, Carbon-containing single-crystal nickel-based superalloys: segregation behavior and carbide formation”, Mat. Sci. Eng., 373A (2004), 50-55.